Supplementary figure

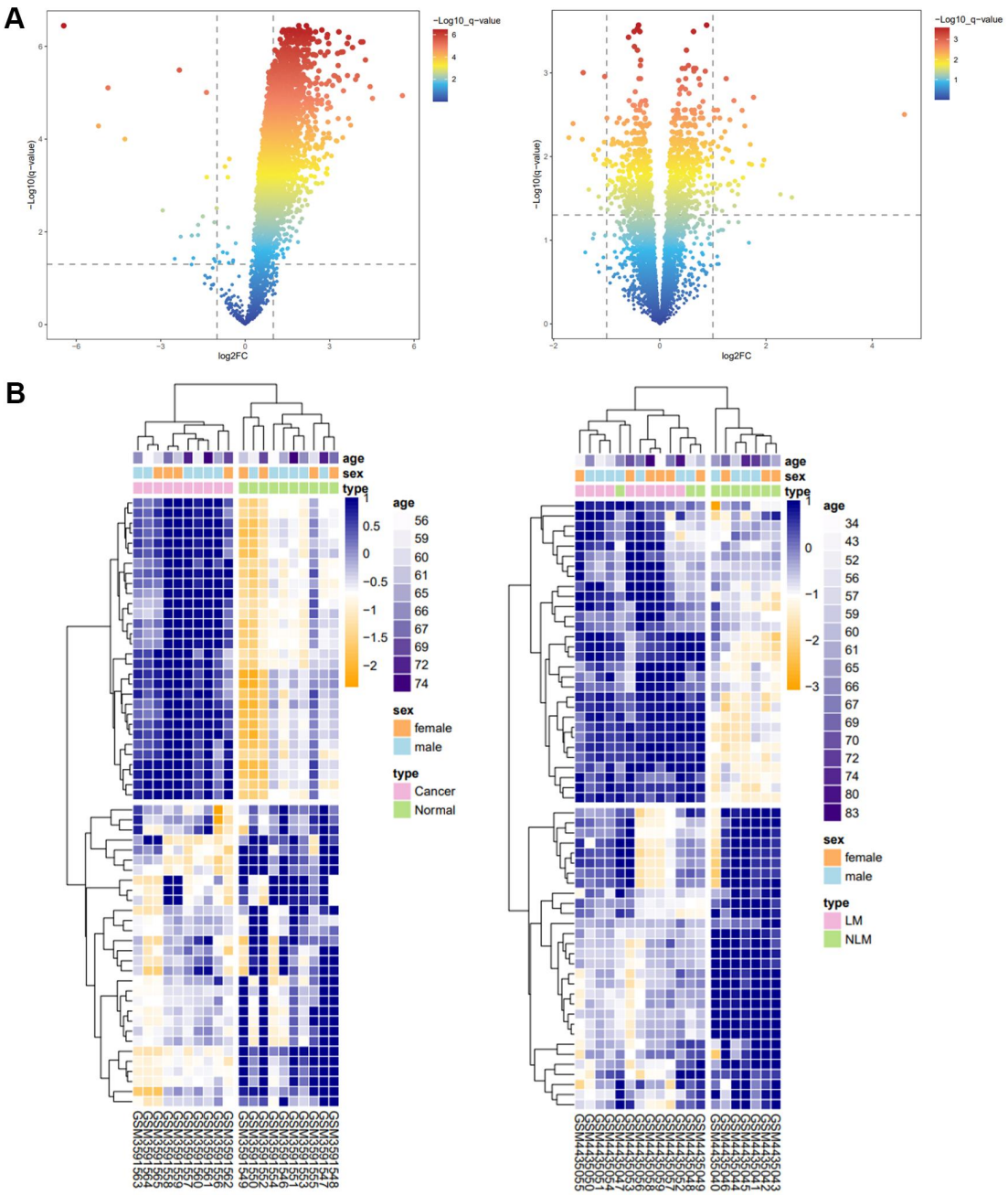

Supplemental Figure 1. CircRNA expression profiles in CRC.

A. A heatmap and volcano plot show the expression of circRNAs in two databases of CRC.

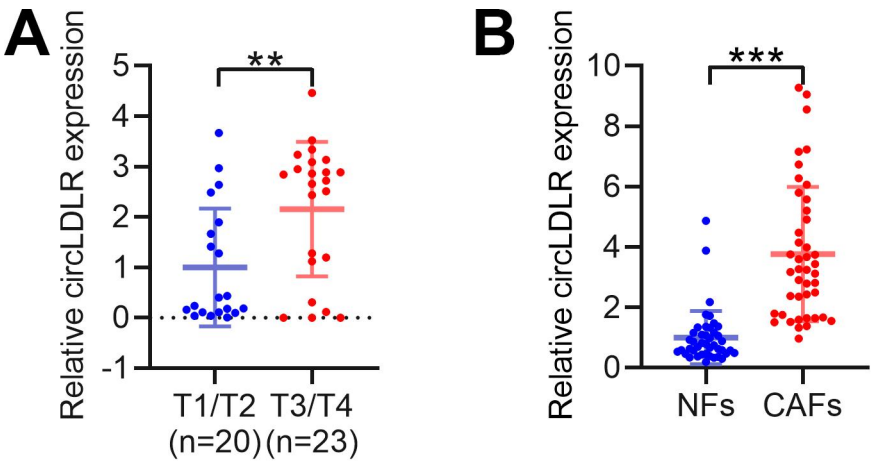

Supplemental Figure 2. The characteristics of circLDLR expression.

A. The relationship between *hsa_circ_0003892* expression and clinicopathologic features in CRC patients. **B.** The expression of *hsa_circ_0003892* was measured by RT-qPCR in CAFs and NFs from 43 paired CRC tissues. ***P*<0.01, ****P*<0.001. Data are presented as mean ± S.D. *P* values are calculated by unpaired two-sided *t*-test.

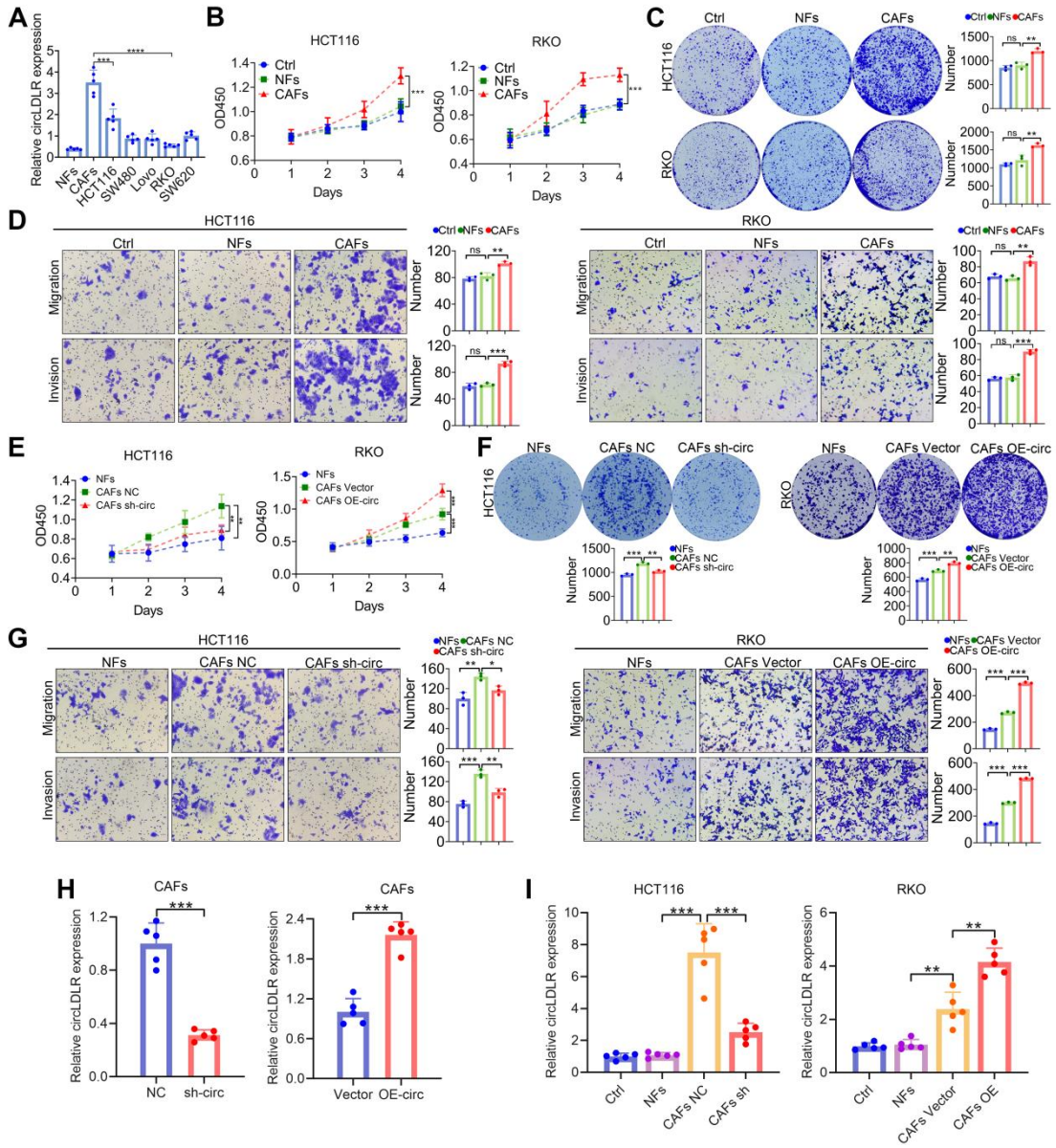

Supplemental Figure 3. The aberrant expression of circLDLR in CAFs exacerbates CRC progression.

A. The relative expression of circLDLR in CAFs, NFs and CRC cells. **B-D.** CCK8, colony formation and transwell were used to evaluate the viability of HCT 116 and RKO cells co-cultured with CAFs and NFs. **E-G.** CCK8, colony formation, and transwell were carried out to detect the growth and invasion of CRC cells co-cultured with indicated CAFs. **H.** The relative expression of circLDLR in CAFs was detected by qRT-PCR. **I.** The relative expression of circLDLR in co-cultured CRC cells was detected by qRT-PCR. ***P*<0.01,****P*<0.001,*****P*<0.0001. In **A**, *n*=5 biologically independent experiments. In **B-G**, *n*=3 biologically independent experiments. Data are presented as mean ± S.D. *P* values are calculated by unpaired two-sided *t*-test.

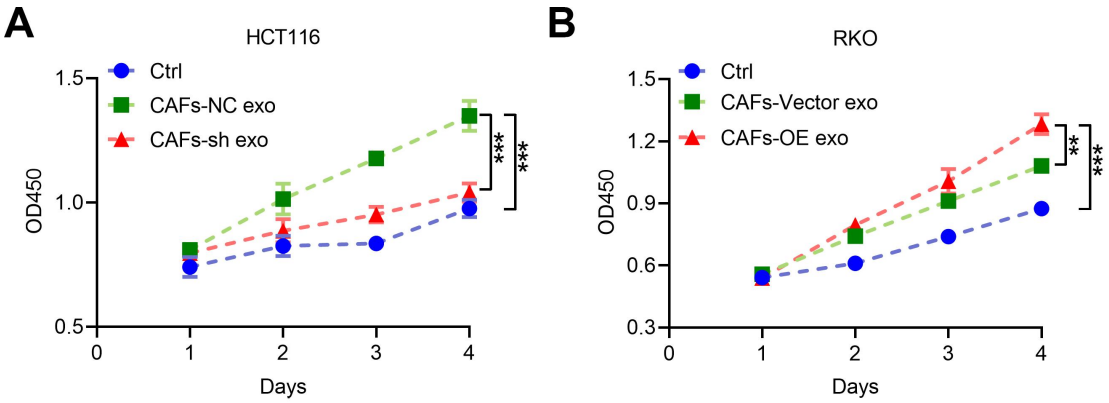

Supplemental Figure 4. The proliferation ability of CRC cells.

A. The proliferation ability of HCT116. **B.** The proliferation ability of RKO. ***P*<0.01, ****P*<0.001. *n*=3 biologically independent experiments. Data are presented as mean ± S.D. *P* values are calculated by unpaired two-sided *t*-test.

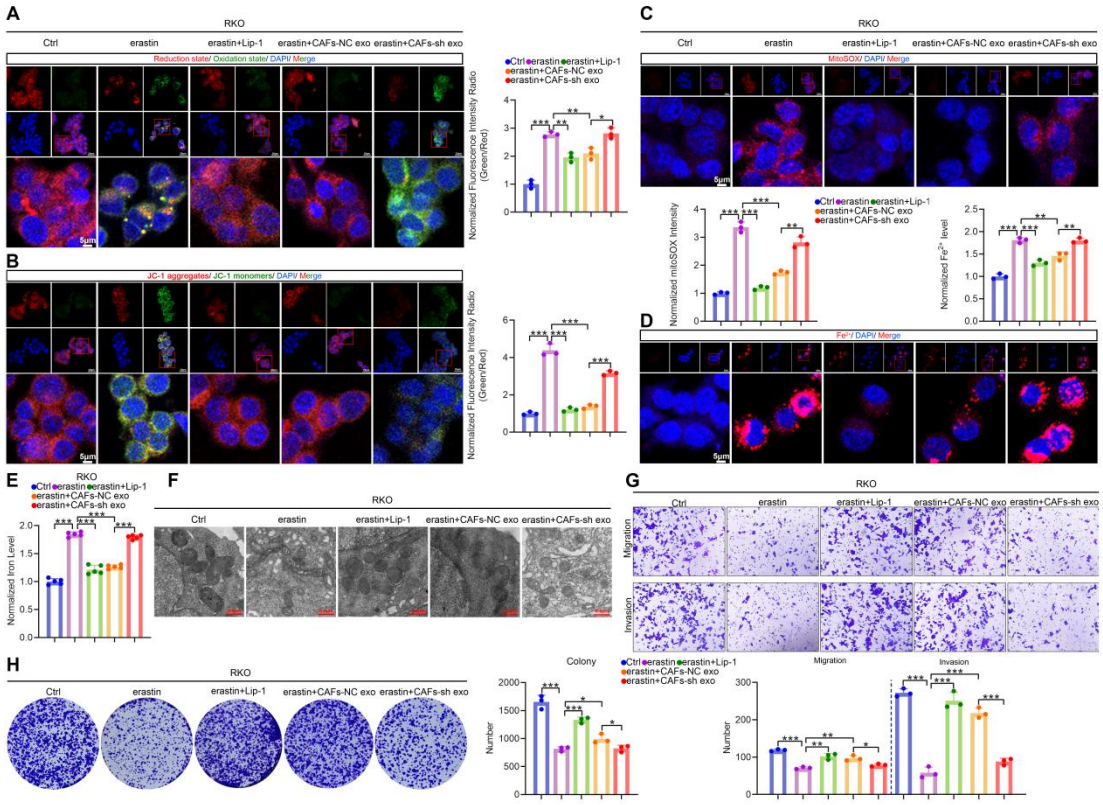

Supplemental Figure 5. CAFs-derived circLDLR facilitates the progression of CRC cells by inhibiting cancer ferroptosis.

A. Lipid peroxidation level in RKO. Scale bar, 5 μm. **B, C.** Relative levels of MMP and MitoSOX. Scale bar, 5 μm. **D, E.** Relative Fe^{2+} and Iron levels. Scale bar, 5 μm. **F.** TEM images of mitochondria. Scale bar, 0.4 μm. **G, H.** Invasion, migration and colony formation assays. **P*<0.05, ***P*<0.01, ****P*<0.001. In E, *n*=5 biologically independent experiments. In **A-D**, **G** and **H**, *n*=3 biologically independent experiments. Data are presented as mean ± S.D. *P* values are calculated by unpaired two-sided *t*-test.

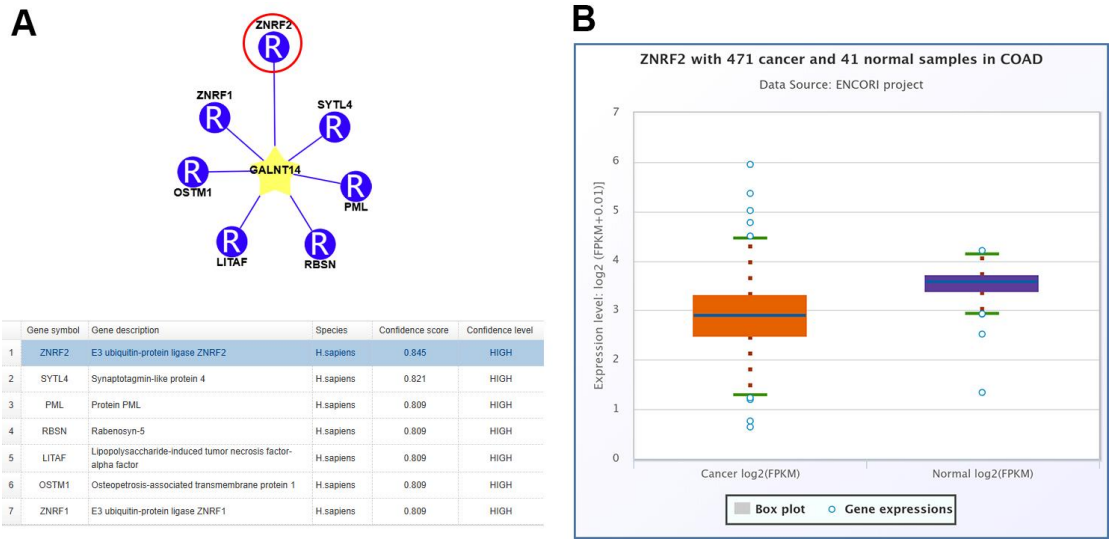

	Gene symbol	Gene description	Species	Confidence score	Confidence level
1	ZNRF2	E3 ubiquitin-protein ligase ZNRF2	H.sapiens	0.845	HIGH
2	SYTL4	Synaptotagmin-like protein 4	H.sapiens	0.821	HIGH
3	PML	Protein PML	H.sapiens	0.809	HIGH
4	RBSN	Rabenosyn-5	H.sapiens	0.809	HIGH
5	LITAF	Lipopolysaccharide-induced tumor necrosis factor-alpha factor	H.sapiens	0.809	HIGH
6	OSTM1	Osteopetrosis-associated transmembrane protein 1	H.sapiens	0.809	HIGH
7	ZNRF1	E3 ubiquitin-protein ligase ZNRF1	H.sapiens	0.809	HIGH

Supplemental Figure 6. The prediction of E3 ubiquitin ligase in GALNT14.

A. The prediction of E3 ubiquitin ligase. **B.** The expression of ZNRF2 in cancer and normal samples.

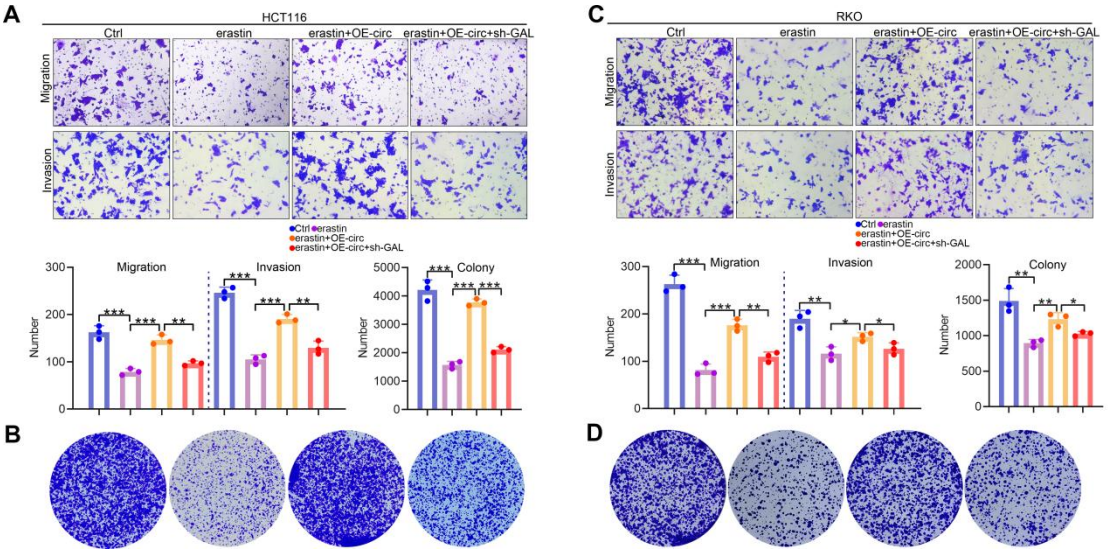

Supplemental Figure 7. The migration, invasion and colony abilities of CRC cells were influenced by circLDLR and GALNT14.

A. Transwell assays of HCT116. **B.** Colony formation of HCT116. **C.** Transwell assays of RKO. **D.** Colony formation of RKO. *n*=3 biologically independent experiments. Data are presented as mean ± S.D. *P* values are calculated by unpaired two-sided *t*-test.

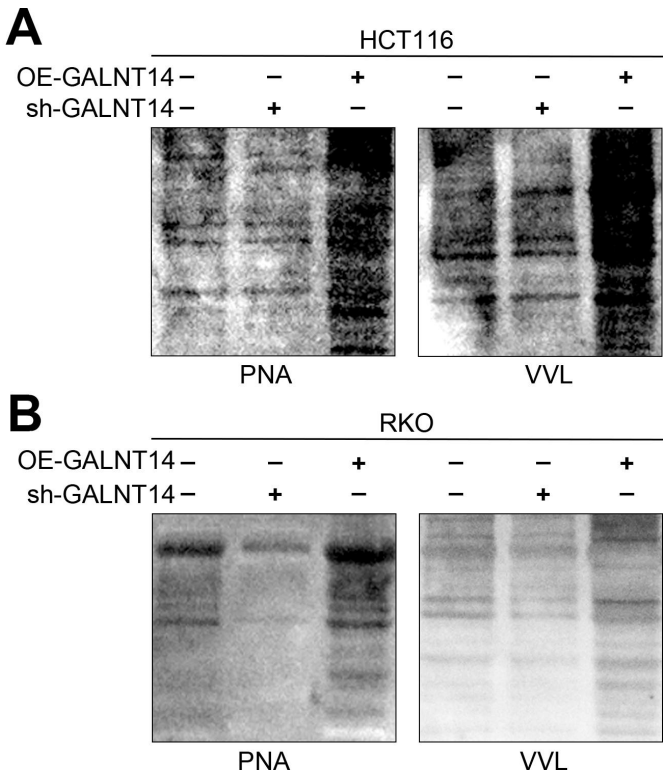

Supplemental Figure 8. GALNT14 enhances total protein O-GalNAcylation in CRC cells.

A, B. Western blot analysis of total protein O-GalNAcylation with GALNT14 overexpression or deletion in CRC cells.

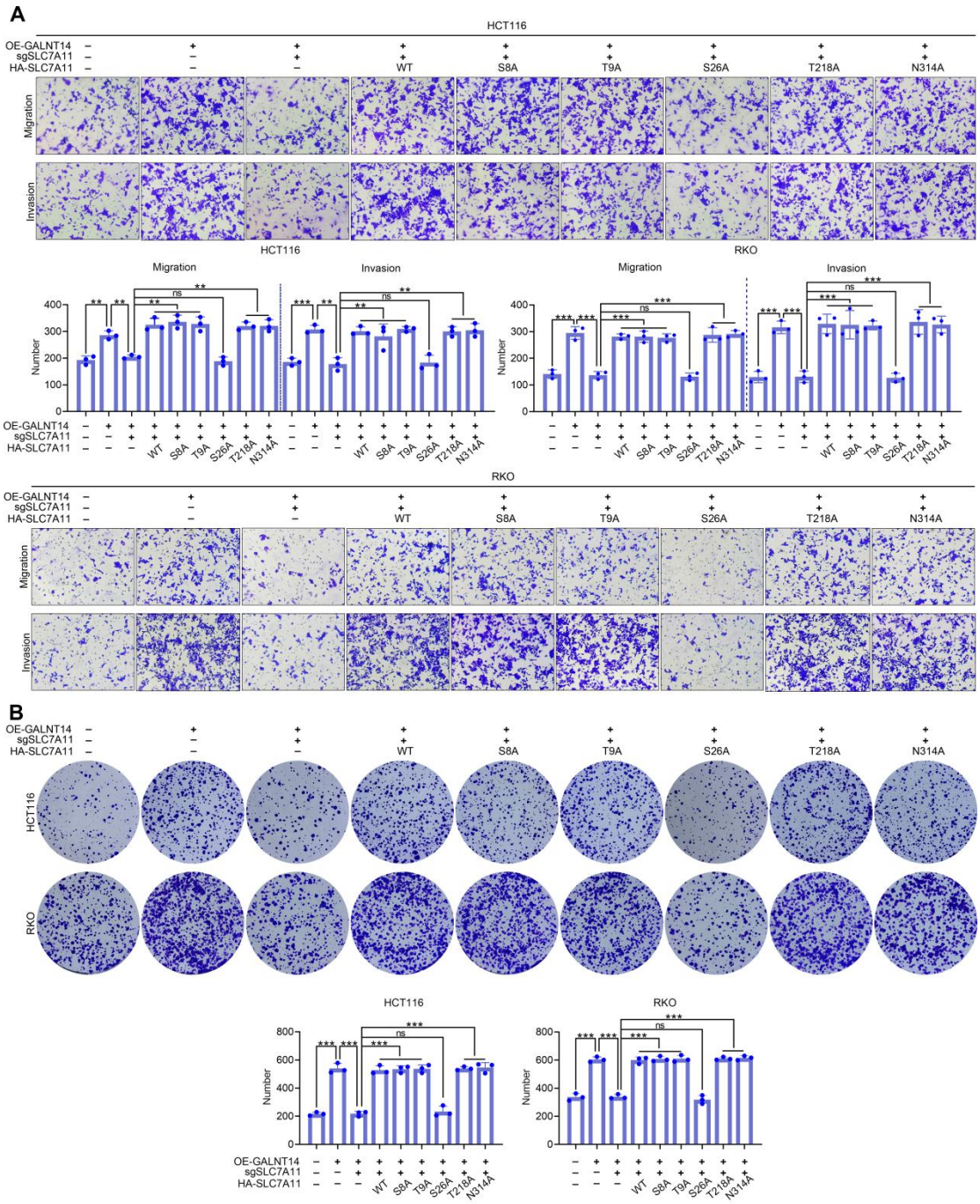

Supplemental Figure 9. The proliferation, migration and invasion abilities of CRC cells.

A. Transwell was used to evaluate the viability of CRC cells. **B.** Colony formation was used to evaluate the viability of CRC cells.

A

Circular RNA	Tag Name	% Identity	Alignment Length	Mismatches	Gap Openings	Tag Start	Tag End	Circular RNA Start	Circular RNA ENd
hsa_circ_0003892	HHLE1_174170_eIF4AIII_rep1_174170_38_86	100.00	85	0	0	2	86	141	225
hsa_circ_0003892	HHLE1_174171_eIF4AIII_rep1_174171_11_46	100.00	46	0	0	1	46	250	295
hsa_circ_0003892	HHLE1_174176_eIF4AIII_rep1_174176_1_36	100.00	35	0	0	2	36	293	327
hsa_circ_0003892	HHLE2_569484_eIF4AIII_rep2_569484_4_36	100.00	36	0	0	1	36	431	466
hsa_circ_0003892	HHLE1_174179_eIF4AIII_rep1_174179_11_78	100.00	77	0	0	2	78	465	541
hsa_circ_0003892	HHLE2_569477_eIF4AIII_rep2_569477_6_65	100.00	65	0	0	1	65	78	142
hsa_circ_0003892	HHLE1_174169_eIF4AIII_rep1_174169_5_51	100.00	51	0	0	1	51	92	142

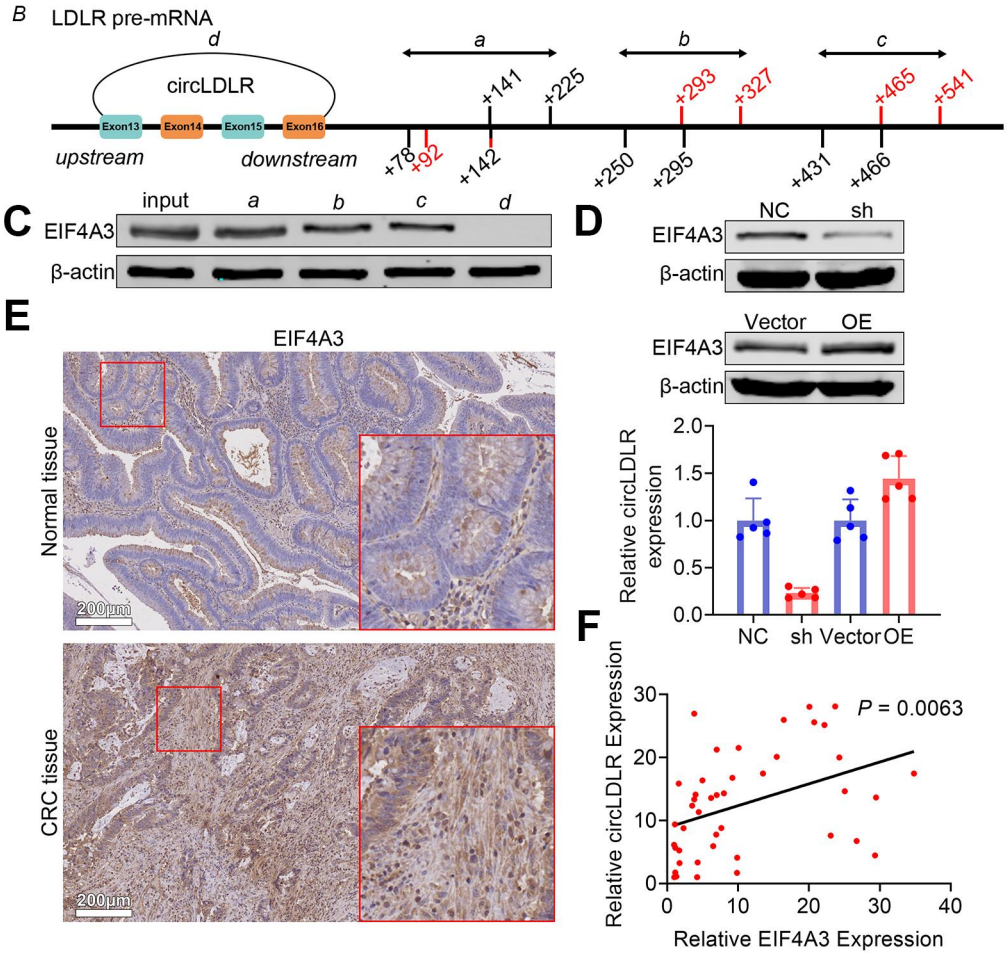

Supplemental Figure 10. Biogenesis of circLDLR is facilitated by EIF4A3.

A. Prediction of the putative EIF4A3 binding sites in circLDLR pre-mRNA by CircInteractome database. **B.** Five positions (*a*-*d*) in circLDLR pre-mRNA. **C.** Western blot analysis of EIF4A3 protein with RNA pulldown assay. **D.** The levels of circLDLR in CAFs transfected with sh-NC, sh-EIF4A3, OE-Vector, OE-EIF4A3. n=5 biologically independent experiments. **E.** Representative images of IHC staining in CRC tissue and adjacent normal tissue. Scale bar, 200 μm. **F.** The relationship between EIF4A and circLDLR in CRC tissues (n=43). *P<0.05,***P<0.001. Data are presented as mean ± S.D. P values are calculated by unpaired two-sided t-test.